ACS APPLIED MATERIALS & INTERFACES

Research Article

www.acsami.org

Formation of Highly Thermostable Copper-Containing Energetic Coordination Polymers Based on Oxidized Triaminoguanidine

Qi-Long Yan,[†,§] Adva Cohen,[†] Natan Petrutik,[†] Avital Shlomovich,[†] Jian-Guo Zhang,[‡] and Michael Gozin*[,†]

[†]School of Chemistry, Faculty of Exact Science, Tel Aviv University, Tel Aviv, 69978, Israel

[‡]State Key Laboratory of Explosion Science and Technology, Beijing Institute of Technology, 100081 Beijing, China

Supporting Information

ABSTRACT: A series of novel highly thermostable energetic coordination polymers (ECPs), with promising mechanical sensitivity properties, were prepared by an in situ oxidation−coordination reaction of triaminoguanidine hydrochloride with copper nitrate in aqueous solution. The molecular structures and properties of these ECPs could be tuned, by varying the ratios and concentrations of the starting materials. Our ECPs exhibit remarkable thermostability (>390 °C) and very low sensitivity to impact (I_m > 98 J). The best-performing material (**ECP-5**) has a calculated detonation velocity of 8969 m·s^{-1} and a decomposition peak temperature of 396.9 °C, demonstrating an outstanding balance between two inherently contradicting properties: high detonation performance and very low sensitivity.

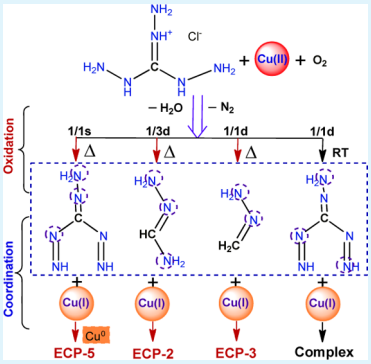

KEYWORDS: *energetic materials, triaminoguanidine, oxidation, thermostable, coordination polymers*

1. INTRODUCTION

Science and technology of energetic materials (EMs), including propellants, explosives, and pyrotechnics, is an important research topic because of the extensive applications of EMs in defense, aerospace industry, mining, and construction.[1] EMs are still under extensive development in terms of new energetic molecules, advanced energetic composites, novel energetic formulations, as well as unique energetic systems.[2,3] There have been a significant amount of new EMs being developed during the past decades, such as new energetic polymers,[4,5] novel nitro compounds,[6] energetic salts,[7] nitrogen-rich compounds, based on azole and azine rings,[8,9] energetic ionic liquids,[10] nanothermites,[11] polynitrogen compounds,[12] and energetic supermolecules, including host−guest complexes, cocrystals, as well as energetic metal−organic frameworks (MOFs).[13−17] However, the newly developed energetic compounds, in most cases, are still incapable of replacing currently used high EMs because of at least one of the following disadvantages: chemical incompatibility, insufficient thermal stability, poor sensitivity, environmental toxicity, and a high production cost. Therefore, energetic supermolecules with tunable properties could be a prospective alternative to solving some of these problems. Recently, MOFs have attracted great attention because of their intriguing molecular topologies and potential applications.[18−20] In particular, energetic MOFs could be synthesized by using certain energetic molecules as linking units, resulting in the formation of highly ordered materials with high heat of detonation, such as the recently reported 1D MOFs, with the formula of $[Ni(NH_2NH_2)_5(ClO_4)_2]_n$ and $[Co(NH_2NH_2)_5(ClO_4)_2]_n$. In another report, hydrazinium perchlorate was used for the preparation of a linear polymeric structure,[21] yielding very powerful metal-based EMs, with detonation heats comparable to those of the state-of-the-art EMs, such as 2,4,6,8,10,12-hexanitrohexaazaisowurtzitane (CL-20; ∼6.28 kJ·g^{-1}). Unfortunately, the above-mentioned energetic MOFs were found to be very sensitive to impact and friction because of the low rigidity characteristics of the linear polymeric chain structures. In order to decrease the mechanical sensitivity, investigators used hydrazinecarboxylate as a ligand for the preparation of energetic coordination polymers (ECPs) with sheet-type structures, including $[(Co_2(N_2H_4)_4(N_2H_3CO_2)_2)(ClO_4)_2\cdot H_2O]_n$ (CHHP) and $[(Zn_2(N_2H_4)_3(N_2H_3CO_2)_2)(ClO_4)_2\cdot H_2O]_n$ (ZnHHP), which showed a considerable decrease in sensitivity, but unfortunately their heats of detonation were low.[22] In comparison, the energetic 3D MOFs possess more variable connection modes, and some of these materials have enhanced structural reinforcement, resulting in their improved thermal stability and energetic performance. Two halogen-free energetic 3D MOFs, $[Cu(atrz)_3(NO_3)_2]_n$ and $[Ag(atrz)_{1.5}(NO_3)]_n$, were recently prepared by using a highly thermostable energetic ligand, 4,4′-azo-1,2,4-triazole (atrz, with a N content of 68.3%), instead of hydrazine.[23,24] Yet, these two 3D MOFs exhibited much lower thermal stability than the parent atrz ligand, which

Received: June 14, 2016
Accepted: August 1, 2016
Published: August 2, 2016

DOI: 10.1021/acsami.6b07165
ACS Appl. Mater. Interfaces 2016, 8, 21674−21682

Table 1. Molecular Compositions, Formulas, Molecular Weights, and Key Atom Ratios in TAG-Cu^{I} Complexes and ECPs[a]

sample	empirical formula	FW		elemental content (wt %) Cu	C	N	Cl	H	O	M.R. C/Cu/Cl[a]	M.R. C/H[b]
ECP-1	$[Cu_2(CN_2H_4)Cl{\cdot}H_2O]_n$	205.0	exptl	31.20	11.92	27.45	17.39	4.23	7.81	2/1/1	1/10
			calcd	31.00	11.72	27.31	17.29	4.88	7.80		
ECP-2	$[Cu_2(CN_3H_5)Cl_2(H_2O)_2]_n$	293.0	exptl	43.62	4.26	14.29	24.42	3.08	10.33	1/2/2	1/9
			calcd	43.38	4.10	14.33	24.20	3.07	10.92		
ECP-3	$[Cu_2(CN_2H_4)Cl_2{\cdot}3H_2O]_n{\cdot}CuCl$	394.0	exptl	48.79	3.01	7.13	26.65	2.32	12.20	1/3/3	1/10
			calcd	48.39	3.05	7.11	26.99	2.28	12.18		
ECP-4	$[Cu_2(CN_2H_4)Cl_3]_n{\cdot}CuCl$	376.5	exptl	50.40	3.24	7.65	37.63	1.08	0.00	1/3/4	1/4
			calcd	50.64	3.19	7.44	37.67	1.06	0.00		
ECP-5	$[Cu(CN_6H_4)Cl)]_n{\cdot}4CuCl{\cdot}2Cu$	722.1	exptl	61.47	1.61	11.91	24.41	0.60	0.00	1/7/5	1/2
			calcd	61.60	1.66	11.63	24.55	0.56	0.00		
TAG-Cu^{I}_1/1d (complex)	$Cu_2(CN_6H_4)Cl_2{\cdot}H_2O$	314.0	exptl	40.31	3.89	26.53	22.51	1.82	4.94	1/2/2	1/4
			calcd	40.22	3.80	26.58	22.44	1.90	5.06		

[a]The FW, formula weight, is calculated from the simplest experimental predicted monomer; TAG-Cu^{II}_1/1d_RT represents the TAG-Cu^{II} complex prepared under room temperature, while the others are ECPs; the M.R., atomic molar ratio, is determined by EDS (a) and EA by burning gaseous products (b). Exptl values for C were obtained by the average values by EDS and EA methods and H were obtained by calculation of the average C content and C/H ratio from EA, while the other values (calcd) were determined from the C/Cu/Cl ratio by EDS and the average C content.

has a decomposition temperature (T_d) of 313 °C, whereas the corresponding 3D MOFs decomposed below 260 °C.[14]

A recent study showed that by using a tetrazole−triazole ligand, 3-(1*H*-tetrazol-5-yl)-1*H*-triazole (H_2tztr), for the preparation of energetic 3D MOFs, the T_d value of these 3D MOFs could be increased to 355 °C, which is higher than that of the parent H_2tztr ligand.[15]

Similar to the above-mentioned azole-based ligands, guanidine and its derivatives represent an additional class of N-donor ligands with basic and nucleophilic functional groups. A combination of various metal ions and guanidine-derived building blocks should allow the building of a combinatorial library of EMs suitable for various applications, where the properties could be tuned by the selection of specific metal ions and nitrogen-rich components.[25−28] Guanidine-based ligands have already been investigated in bioinorganic chemistry,[29−31] as well as in the preparation of copper-based catalysts for atom-transfer radical polymerization (ATRP).[32,33] For instance, certain guanidine derivatives may contain additional N-donor moieties, such as pyridine or quinoline.[34,35] It was reported that the multifunctional guanidines could promote changes in the oxidation state of Cu ions, from Cu^{I} via Cu^{II} to Cu^{III}. This property of guanidine ligands, to stabilize metal centers with various oxidation states, makes them outstanding ligands for homogeneous catalysis. Several studies have been reported regarding the preparation of diaminoguanidine (DAG) copper complexes, such as $Cu(DAG)(NO_3)_2$, $Cu(DAG)_2(NO_3)_2$, and $Cu(DAG)_2(NO_3)_2{\cdot}HNO_3$. In the latter complex, both the neutral DAG and DAG^+ cation are bound to Cu, the crystal structure of which is similar to that of $[Cu(DAGH)Cl_3]$.[36−39] Despite all of this prolific activity, the energetic properties of guanidine-based metal complexes were never reported.

In general, guanidine derivatives are very energetic, and among them, triaminoguanidine (TAG and its nitrate salt) has the highest N content. The TAG moiety could be used as a promising ligand or cation for the preparation of various energetic coordination compounds and ionic liquids.[40,41] There are only two known examples of TAG-Cu complexes. The first reported example describes the reaction between $Cu(NO_3)_2$ and TAG·HNO_3, conducted in aqueous solution (pH = 1, at room temperature), yielding a $Cu(TAG)(NO_3)_2$ complex.[38] The second complex, containing protonated TAG, was prepared by the reaction of equimolar amounts of $CuCl_2$ and TAG·HCl, in concentrated aqueous HCl (at room temperature).[39] We discovered that, at elevated temperatures, the reaction between $Cu(NO_3)_2$ and TAG·HCl, in aqueous solution, led to a rich new chemistry and to the formation of much more intricate and unique materials. At higher temperatures, in the presence of Cu^{II} ions, the TAG ligand undergoes oxidation and coordination processes, forming either a copper complex or energetic coordination polymers (ECPs). More importantly, the structures of the obtained ECPs are highly dependent on the molar ratios of the reactants. It was further shown that some of the ECPs have superior energetic properties and much higher thermostability than the previously reported azole-based 3D MOFs.[15]

2. EXPERIMENTAL SECTION

2.1. Preparation of ECP-1, ECP-2, and ECP-3 (in a Diluted Solution of Copper Nitrate). An aqueous solution of TAG·HCl (20 mL, 250 mM) was added to a stirred (900 rpm) aqueous solution of $Cu(NO_3)_2{\cdot}3H_2O$ (100, 200, or 300 mL, 50 mM) at 65−75 °C, and the reaction mixture was kept at this temperature for 2 h. After that time, the formed precipitate [TAG-Cu^{I}_1/1d (**ECP-1**), TAG-Cu^{I}_1/2d (**ECP-2**), and TAG-Cu^{I}_3/1d (**ECP-3**), respectively] was filtered, washed with water, and vacuum-dried for several days (color changes during the drying process indicate dehydration of the prepared materials; Figure S1).

2.2. Preparation of ECP-4, ECP-5, and Related Materials (in a Concentrated Solution of Copper Nitrate). An aqueous solution of TAG·HCl (20 mL, 250 mM) was added to a stirred (900 rpm) aqueous solution of $Cu(NO_3)_2{\cdot}3H_2O$ (25, 20, 15, 10, 5, and 2.5 mL, 500 mM) at 70−80 °C, and the reaction mixture was kept at this temperature for 2 h. After that time, the formed precipitate [TAG-Cu^{I}_1/5s, TAG-Cu^{I}_1/4s, TAG-Cu^{I}_1/3s, and TAG-Cu^{I}_1/2s (**ECP-4**), TAG-Cu^{I}_1/1s (**ECP-5**), and TAG-Cu^{I}_2/1s, respectively] was filtered, washed with water, and vacuum-dried for several days (color changes during the drying process indicate dehydration of the prepared materials; Figure S1).

2.3. Preparation of the TAG-Cu^{I} Complex..[38,39] An aqueous solution of TAG·HCl (20 mL, 250 mM) was added to a stirred (900 rpm) aqueous solution of $Cu(NO_3)_2{\cdot}3H_2O$ (20 mL, 250 mM) at 25−35 °C, and the reaction mixture was kept at this temperature for 2 h. After that time, the formed precipitate TAG-Cu^{I} complex was filtered, washed with water, and vacuum-dried.

DOI: 10.1021/acsami.6b07165
ACS Appl. Mater. Interfaces 2016, 8, 21674−21682

Comprehensive characterization of all prepared materials is presented in the Supporting Information (SI).

3. RESULTS AND DISCUSSION

3.1. Elemental Analysis (EA) of ECPs. The resulting ECPs had different colors and morphologies (Figure S1). We found that **ECP-1**, **ECP-3**, **ECP-4**, and **ECP-5** are very stable, while **ECP-2** is slightly hygroscopic (see the SI). These ECPs were isolated as microcrystalline powders and found to be practically insoluble in all common organic solvents and water. The difference in the colors of our ECPs most probably results from variations in their molecular structures. Table 1 summarizes the results of EA conducted for the TAG-Cu^{I} complexes and their corresponding ECPs. The elemental content of our materials was determined on the basis of a combination of three different analytical techniques, including combustion EA, energy-dispersive spectroscopy (EDS), and X-ray photoelectron microscopy (XPS). It is clear from the results presented in Table 1 that the original TAG ligand, which has a N/C ratio of 6/1, undergoes partial decomposition during the formation of various ECPs because in the latter materials the N/C ratio is typically less than 6/1. In contrast, the Cu contents in these ECPs are very different, although the Cu/Cl ratio was maintained at 1/1. These findings strongly indicate that the TAG ligand underwent an oxidation reaction that was promoted by Cu^{II}, forming various Cu^{I}-containing ECPs. Cu^{II}-induced oxidations are well-known in organic synthesis,[42] and the oxidation of TAG, in the presence of transition-metal ions, was also reported, where two possible oxidation mechanisms were suggested (Scheme S1).[43] In the absence of the possibility of measuring single-crystal X-ray diffraction (XRD), because of the lack of solubility of our ECPs, the most plausible molecular structures of these materials and their crystal morphologies were determined using a combination of XPS, Fourier transform infrared (FTIR), powder X-ray diffraction (PXRD), and scanning electron microscopy (SEM) techniques.

3.2. Chemical Bonding in ECPs. The chemical structures of nitrogen-rich ligands in our ECPs were evaluated by FTIR and XPS analysis (Figures 1, 2, and S2), with summarized peak assignments presented in Tables S1 and S2. The types of chemical bonds in the TAG-Cu^{I} complex and ECPs, as well as in their precursors, were also determined (see sections 2.1 and 2.2 in the SI). It has been unambiguously shown that N atoms in the ligands are coordinated with Cu^{I} in all of these materials.

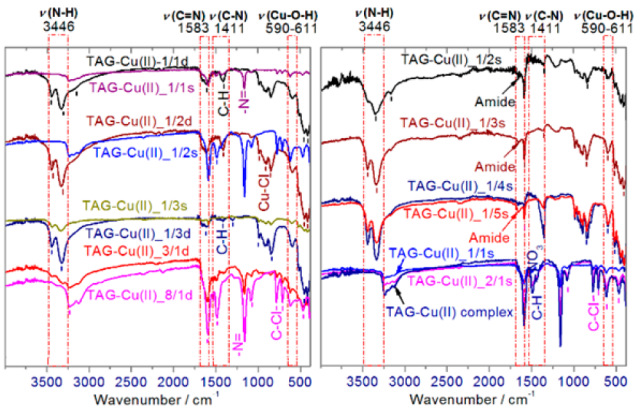

Figure 1. FTIR spectra of the TAG-Cu^{I} complex and selected ECPs, prepared under different reaction conditions.

The H_2O molecule and one of Cl^{-} or NO_3^{-} ions were also found to be in coordination with Cu metal centers.

Our FTIR results indicated a lack of primary amine groups present in the spectra of several materials, including **ECP-5**, TAG-Cu^{I}_2/1s, **ECP-1**, and TAG-Cu^{I}_8/1d, while peaks that were assigned to the C−N═NH group could be clearly detected in the spectra os these materials. Also, from FTIR spectral analysis of **ECP-2** and **ECP-3**, we concluded that C−H bonds were formed in these materials, following TAG oxidation. This conclusion was consistent with our XPS results for **ECP-2** and **ECP-3**, where C 1s peaks of these two materials showed a much higher intensity of C−H/C−C bonds (Figures 2 and S3). Although there are small C 1s peaks that could be attributed to the presence of the C−C bond in the complex and **ECP-5**, we could not postulate the presence of this bond in structures of these materials because of a lack of C−C bond peaks in the FTIR spectra of the complex and **ECP-5**. It should be noted that frequently, in samples that were exposed to air, C 1s peaks of C−C, C−O−C, and O−C═O components could be found because of the presence of organic contaminants in the air.

Our XPS measurements also revealed that, in the case of **ECP-2**, C is covalently bound to a Cu^{I} metal center, whereas one additional amino group is bound to C in **ECP-1** and **ECP-2**. No C−Cu bond was observed in the XPS spectra of the two latter materials (Figure S3).

As ligands, TAG and its oxidized products have C 1s peaks corresponding to C−N (285.7−286.0 eV) and C═N (286.5−286.7 eV) bonds, as well as N 1s peaks corresponding to ═N− (398.4 eV) and −NH− (399.7 eV) bonds. These peak intensities depend on the oxidation state.[44−47] The observed N 1s binding energy for −NH− at 400.1 or 400.2 eV (Table S2) is in agreement with the reported values for organic amines, which are coordinated to metal ions (in the solid state).[45] The presence of a positively charged N atom could be the result of an amine N−Cu bond, while the negatively charged N atom could be due to the presence of a C−Cu bond, which was only found in N 1s XPS spectra of **ECP-2**.[46] In general, two Cu $2p^{3/2}$ peaks at 934.9 and 944.2 eV could be attributed to copper(II) compounds, while the peak at 932.4 eV corresponds to the Cu^{I}−N bond in our compounds. The latter peak is usually overlapped with the peak of metallic copper (Cu^{0}).[47] In XPS spectra of all tested ECPs, the peaks corresponding to the Cu^{I}−N bond were found to be dominant, except the spectrum of **ECP-2**, in which the Cu^{I}/Cu^{II} peak intensity ratio was almost 1/1. This indicates the presence of both Cu^{I}/Cu^{II} metal centers in this material. We also noticed that, in the case of **ECP-5**, the peak ratio of Cu^{I} (or Cu^{0}) to Cu^{II}, in its XPS spectrum, was much higher than those for all other materials that were prepared in this study, suggesting the presence of Cu^{0}. This conclusion was further supported by the PXRD analysis conducted for this material (Figure S4). The coordination behavior of N sp^2 donors in ligands, which are TAG oxidation products, is similar to that of azoles, where each N-donor atom of azolate generally coordinates only to one transition-metal center.[48] On the basis of the EA results, in complexes **ECP-2** and **ECP-3**, H_2O molecules were found in the structures of these materials, while in the cases of **ECP-1**, **ECP-4**, and **ECP-5**, no presence of H_2O ligands was detected (Figures 2 and S6).

3.3. Proposed Molecular Structures of ECPs and Their Formation Mechanisms. It was previously reported that the chemical instability of TAG ligands could be improved by their modification with certain functional groups, such as benzyl and

DOI: 10.1021/acsami.6b07165
ACS Appl. Mater. Interfaces 2016, 8, 21674−21682

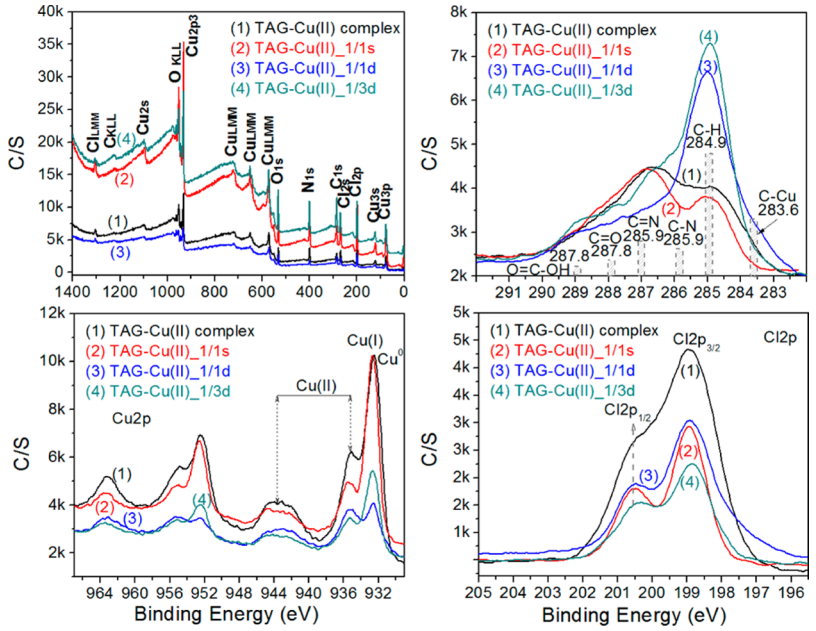

Figure 2. XPS spectra of the TAG-Cu^{I} complex and selected ECPs that were prepared at various molar ratios of the starting materials (in 1/1 and 1/3 molar ratios).

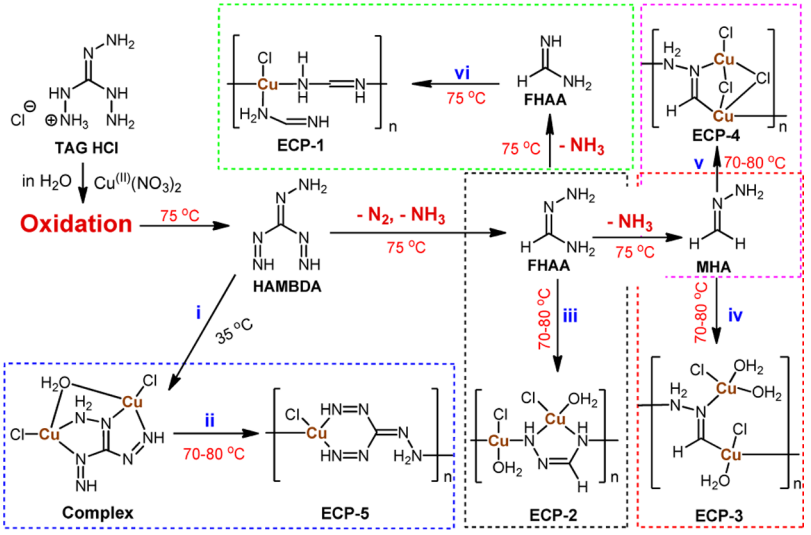

Figure 3. In situ oxidation of TAG promoted by Cu^{II} and coordination reactions between HAMBDA, FHAA, and MHA and Cu^{I} ions, leading to formation of the corresponding ECPs. The reaction outcome is significantly dependent on the reaction conditions [the molar ratio of TAG/Cu^{II} for reactions (i) and (ii) was 1/1 in diluted and saturated solutions, respectively; the ratios were 1/1 and 1/3 for reactions (iii) and (iv) in a diluted solution, respectively; the ratio was 1/2 for reaction (v) in a saturated condition and 3/1 for reaction (vi) in a diluted solution; a trace amount of metallic copper was also observed in the cases of saturated reaction solutions, with reactant TAG/Cu^{II} ratios greater than 1/1].

its derivatives.[44] On the basis of the above-mentioned elemental composition and chemical bond analyses, plausible reaction passageways and corresponding oxidation mechanisms could be envisioned in the formation of our ECP materials (Figure 3). We believe that three ligands, including hydrazonomethylenebis(diazene) (HAMBDA), (*Z*)-formohydrazonamide (FHAA), and methylene hydrazine (MHA), and their corresponding ECPs are formed during the Cu^{II}-promoted oxidation of TAG at an elevated temperature of about 75 °C (e.g., **ECP-2**, **ECP-3**, and **ECP-5**; Figure 3). In contrast, at room temperature (and up to 35 °C), the oxidized TAG-Cu^{I} complex is formed. Under elevated temperature reaction conditions, it was possible to control the structure of the resulting ECPs by using certain concentrations of starting materials in aqueous solution and by altering the TAG/Cu^{II} ratios. Our EA results indicated that Cu ions in the TAG-Cu^{I} complex are coordinated in a binuclear mode, while the ECPs have either binuclear copper repeating units (**ECP-2**, **ECP-3**, and **ECP-4**) or mononuclear monomers (**ECP-1** and **ECP-5**). In comparison, benzyl derivatives of TAG, as tridentate ligands, form equilateral triangular complexes of coordinated metal ions, which were further utilized for the preparation of high-nuclearity complexes and coordination polymers.[51,52] In our case, copper ECP materials based on FHAA and MHA ligands exhibit lower molecular-level porosity and higher thermostability than somewhat larger nitrogen-rich energetic ligands

DOI: 10.1021/acsami.6b07165
ACS Appl. Mater. Interfaces 2016, 8, 21674−21682

(used for the preparation of ECPs), such as H2tztr and atrz ligands.

3.4. Prediction of the Crystal Structures of ECPs by PXRD. The crystal structures of all ECPs obtained in this study were analyzed by PXRD (Figure S4), and their diffraction patterns were compared to the patterns of TAG·HCl and the TAG-Cu^{I} complex. We found that the diffraction patterns of ECPs and the complex were different in peak numbers, positions, and intensities (Tables S3–S12). The patterns were indexed, and the corresponding space groups were determined, based on unit-cell refinement and by using the *JADE* software (Table S13). Our PXRD data (Figures 4 and S4) showed no

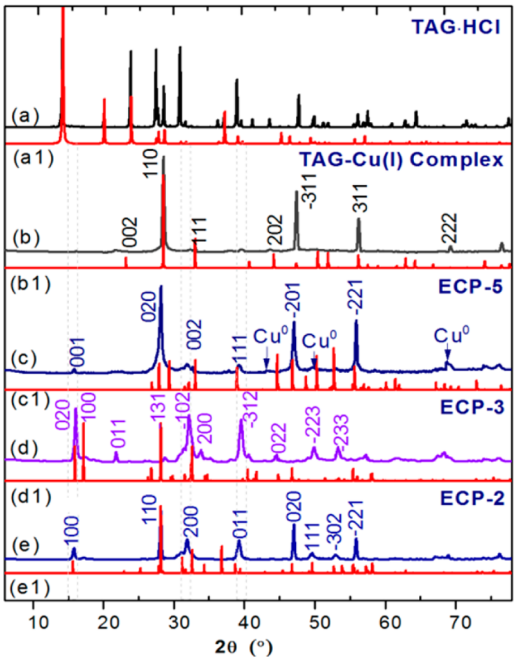

Figure 4. Comparison of the experimental PXRD spectra (**a**-**e**) and the simulated ones for TAG-Cu(I) complex and the typical ECPs (**a1**-**e1**) based on the predicted crystal unit cell parameters (Table S14, ESI).

exact match to any known phases in the ICDD database, while only three peaks matched the metallic copper (Cu^{0}; Figure 4c) for ECPs that were prepared under saturated reaction conditions (e.g., **ECP-5**). It should be noted that, in the cases of **ECP-2** and **ECP-5**, we found that three peaks (at 2θ = 28.58°, 47.56°, and 56.40°) matched the Nantokite CuCl (PDF01-0793) material. Clearly, all our new ECP materials exhibited a distinct crystalline phase that was significantly different from those of both of its $Cu(NO_3)_2$ and TAG·HCl precursors.

All of the above-mentioned data are in very good agreement with the molecular compositions determined by EA (Table 1), e.g., TAG-Cu^{I} complex, $Cu_2(CN_6H_4)Cl_2{\cdot}H_2O$; **ECP-2**, $[Cu_2(CN_3H_5)Cl_2{\cdot}2H_2O]_n$; **ECP-5**, $[Cu(CN_6H_4)Cl)]_n$; and **ECP-3**, $[Cu_2(CN_2H_4)Cl_2{\cdot}3H_2O]_n$.

TAG·HCl was found to crystallize in the hexagonal space group *P*63/*m* (Figure S6),[49,50] while the TAG-Cu^{I} complex and all of the ECPs crystallized in a monoclinic space group (Table S13). In particular, the crystal lattices of the TAG-Cu^{I} complex, **ECP-3**, and TAG-Cu^{I}_8/1d and TAG-Cu^{I}_1/3s follow a symmetry of *P*21/*c* (No. 14), while it was found to be *Cc* (No. 9) for the TAG-Cu^{I}_1/2s and TAG-Cu^{II}_1/2d. The crystal symmetries of **ECP-2** and **ECP-5** are *P*1 (No. 1) and *C*2 (No. 5), respectively. The crystallographic data for these materials are listed in Table S13, while the Miller indexing and corresponding plane distances are summarized in Table S14 (determined from PXRD-fitted peak data by using the *JADE* software).

The TAG-Cu^{I} complex crystal has the space group *P*21/*c*, with cell parameters of a = 6.8581(4) Å, b = 3.6173(1) Å, c = 8.3926(2) Å, β = 98.765(5)°, $\alpha = \gamma$ = 90°, and V = 189.42(3) $Å^3$ with Z = 4. The structure of this complex is square-pyramidal, in which a chlorine ligand is located in the axial position, similar to the structure of the $Cu(DAGH)Cl_3$ complex (Figure S5). The $Cu(DAGH)Cl_3$ complex crystallizes in a monoclinic space group with symmetry of *P*21/*n* (Z = 2).[36] In comparison, the reported six-coordinated TAG-Cu^{II} complex, prepared in concentrated HCl (using $CuCl_2{\cdot}2H_2O$ as the starting material), has the formula $[Cu(TAGH_2)Cl_3]Cl{\cdot}H_2O$ and crystallizes in the orthorhombic space group, with unit cell parameters of a = 10.070(2) Å, b = 11.603(2) Å, c = 18.390(4) Å, and V = 2148.7(7) $Å^3$ in *Pbca* symmetry (Z = 8 and D_{calc} = 2.04 $g{\cdot}cm^{-3}$).[39] It has been shown that the crystal structure of this complex is composed of $[Cu(TAGH_2)Cl_3]^{+}$ cations, Cl^{-} anions, and H_2O molecules. The complex cation is comprised of the coordinated TAG^{2+}, which is bound to the Cu^{II} ion via N atoms of the amino group and via the C–N moiety, in a bidentate chelating mode. The square-planar arrangement of the Cu atom is formed by two Cl atoms (2.277 and 2.300 Å) and two N atoms (Cu–N 1.987 and 2.043 Å).

In the case of the TAG-Cu^{I} complex, each ligand is coordinated with two Cu atoms, and a similar square-planar arrangement is formed for each one of them by one Cl atom and a shared O atom of the H_2O ligand (Figure S6a). The bond lengths of Cu–O(H_2) are comparable to each other (1.95–1.99 Å), while for the Cu–Cl and Cu–N bonds, the lengths are at 1.97–2.20 and 1.75–2.08 Å, respectively. Usually, an increased electron delocalization could be observed in protonated TAG because of the three strong intramolecular hydrogen bonds that accounted for the extra stability of TAG.[40,41] However, the TAG ligand in our complex was oxidized instead of being protonated. More detailed information regarding the obtained crystal structures is presented in Figure S6. In order to generate the proposed crystal structures, *Materials Studio* software was utilized in order to simulate the crystal structures of our ECPs, using the above-mentioned information on the topologies and unit-cell parameters. The simulated PXRD patterns were compared with the experimental ones (Figures 4 and S4), showing a perfect match in the peak position for the TAG-Cu^{I} complex. Minor differences observed for the pattern intensities of **ECP-2** and **ECP-5** can be explained by the fact that the predicted structures were modeled without including the Cu^{0} and CuCl impurities, the presence of which was indicated by the EA and PXRD results.

3.5. Crystal Morphologies of ECPs. SEM images and corresponding EDS spectra of our materials are shown in Figure 5. The **ECP-3**, **ECP-4**, and **ECP-5** samples exhibit a regular 2D flake structure, while the TAG-Cu^{I} complex and **ECP-1** form sphere-shaped structures, with rough surfaces. There are a large number of cavities/defects in the spherical particles of the complex, as shown by its back-scattered electron (BSE) image (Figure S7). However, in the case of **ECP-1**, the crystal particle is a homogeneous solid, due to polymerization, resulting in a higher crystal density.

DOI: 10.1021/acsami.6b07165
ACS Appl. Mater. Interfaces 2016, 8, 21674–21682

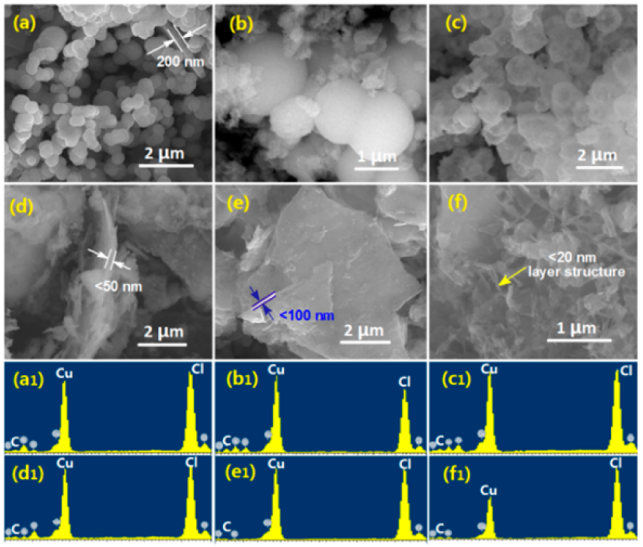

Figure 5. SEM images (a–f) and corresponding EDS spectra (a_1–f_1) of the TAG-Cu^I complex (a) and ECPs (b–f) showing different morphologies and elemental compositions because of changes in the experimental conditions for their preparation. The nanocrystals of the TAG-Cu^I complex (a) prepared at room temperature have a round shape, with rough surfaces and diameters of <500 nm, where the ECP flakes, with thicknesses of ~200 nm are formed as side products. **ECP-1** (b) shows a smooth microsphere shape, with a diameter of ~1.0 μm (conditions, 3/1d), a typical well-oriented 1D ECP; **ECP-2** (c) exists in an amorphous polymeric state (conditions, 1/1d); **ECP-3** (d), **ECP-4** (e), and **ECP-5** (f) exist in layered arrangements, with different thicknesses.

It was also found that, under reaction conditions at which saturated solutions of starting materials were used, the ECPs with 2D flake-type structures, with a thickness of 20–100 nm, were formed, while under the diluted conditions, spherical structures, with diameters of less than 2 μm, were obtained [when the molar ratios between the TAG·HCl and $Cu(NO_3)_2 \cdot 3H_2O$ starting materials were over 3/1].

The Brunauer–Emmett–Teller specific surface areas (SSAs) of the materials in this work were measured using a single-point method (SPM; for P/P_0 = 0.20) and a multiple-point method (MPM), in order to test their porosity and support morphological studies.[53] The largest SSA value of 11.83 $m^2 \cdot g^{-1}$ was determined for the TAG-Cu^I complex by the SPM. SSA values of 4.15, 6.52 (7.43 $m^2 \cdot g^{-1}$ for the MPM), 3.82, and 3.59 $m^2 \cdot g^{-1}$ were determined for **ECP-1**, **ECP-3**, **ECP-4**, and **ECP-5**, respectively (section 1.3 in the SI). In general, for our ECPs, the difference between the SSA values by the SPM and MPM techniques was found to be in a range of about 15%. The relatively low SSA values that were observed for our ECPs demonstrate their nonporous nature and relatively high density of molecular packing (e.g., thin-layered **ECP-5**).

3.6. Thermostability and Reactivity of ECPs. The thermostability and heat flow property are the two key factors that determine the potential applications of our ECPs as EMs. The thermal behavior of the TAG-Cu^I complex and of our most promising ECPs (**ECP-2**, **ECP-3**, and **ECP-5**) was analyzed by both differential scanning calorimetry (DSC) and thermogravimetric analyses (TGA; Figure 6), whereas DSC thermograms for other ECPs are shown in Figure S8. The decomposition peak temperatures of **ECP-2**, **ECP-3**, and **ECP-5** are 421.5, 411.6, and 396.9 °C, respectively, and are much higher than that of the TAG-Cu^I complex (167.8 °C), of the widely used thermostable HMX (287 °C) explosive, and of the known energetic MOFs.[14−16] Interestingly, the thermostability of the TAG-Cu^I complex is even worse than that of TAG·HCl. **ECP-2** and **ECP-5** have comparable heat release characteristics, with a decomposition enthalpy of about 1580 $J \cdot g^{-1}$. **ECP-4** exhibits very low heat release because of the larger amount of CuCl impurity, which was also the case for the other materials prepared from a saturated $Cu(NO_3)_2$ solution, with reactant ratios of TAG/Cu^{II} of less than 1/2 (Figure S8a). Higher Cu^{II} concentrations in reaction solutions ensure higher Cu contents in the formed ECPs, where Cu is functioning as a catalytic center that promotes a thermolysis process. We believe that the catalytic activity of the Cu metal center is the main reason that the exothermic peaks in DSC of **ECP-2**, **ECP-3**, and **ECP-5**, which have higher Cu content than other materials in this study, are much sharper than the exothermic peaks in other ECPs. After the main exothermic decomposition, there are

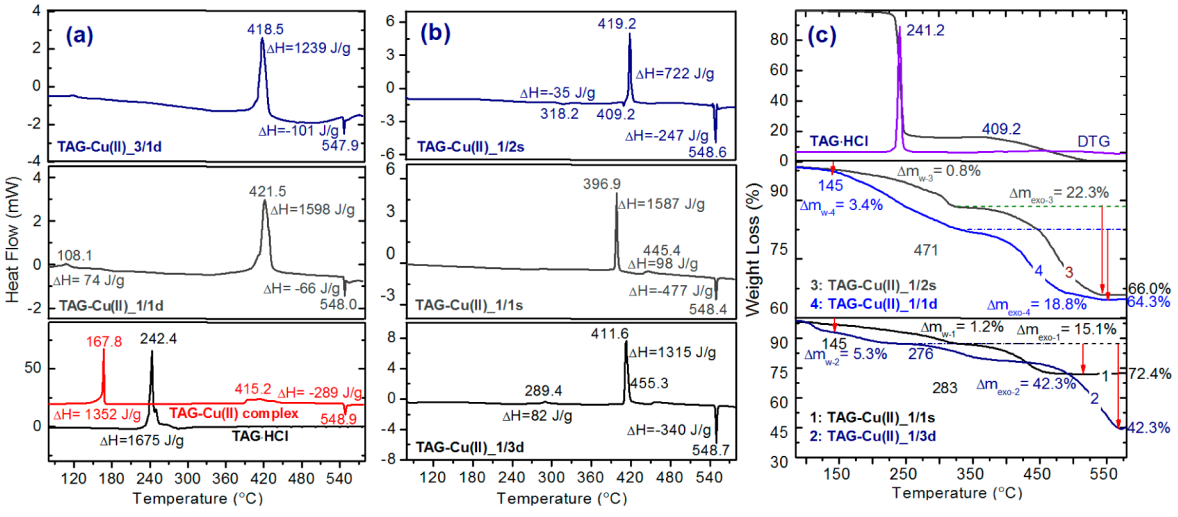

Figure 6. DSC (a and b) and TGA/DTG (c) thermograms of TAG·HCl and selected ECPs, measured at a heating rate of 10 °C·min^{-1}, with sample masses of 0.2–0.3 mg for DSC and 2.0 mg for TGA. The TAG-Cu^I complex decomposes with a fast heat release of below 165 °C (T_p = 167.8 °C), while ECPs are much more thermostable, with fast exothermic decomposition at over 360 °C.

DOI: 10.1021/acsami.6b07165
ACS Appl. Mater. Interfaces 2016, 8, 21674–21682

Table 2. Formula, Color, Physical Properties, and Detonation Performances of the TAG-Cu^{I} Complex and Selected ECPs[a]

sample	formula	physical state	d	Gs	η	T_p	I_m (J)	F (N)	H_f	VoD
TAG·HCl	CH_8N_6HCl	cream white	1.55	80.4	96.4	242.4	25.0	230	+200.2	7.198
TAG-Cu^{I} complex	$Cu_2(CN_6H_4)Cl_2·H_2O$	black spheres	3.01	20.2	94.0	167.8	36.0	>360	−604.2	3.783
ECP-2	$[Cu_2(CN_3H_5)Cl_2·2H_2O]_n$	brown blocks	3.08	34.6	95.6	421.5	>98	>360	−358.9	5.557
ECP-3	$[Cu_2(CN_2H_4)Cl_2·3H_2O]_n$	earth yellow plates	3.12	21.7	91.4	411.6	>98	>360	−482.7	5.926
ECP-5	$[Cu(CN_6H_4)Cl]_n$	dark green plates	3.14	13.5	81.4	396.9	>98	>360	+584.6	8.969
TATB	$C_6H_6N_6O_6$	yellow crystals	1.93			350.1	>98	>360	−154.2	7.350
FOX-7	$C_2H_4N_4O_4$	brown crystals	1.89			238.0	15.0	>200	−188.9	8.870
Cu(atrz)	$[Cu(atrz)_3(NO_3)_2]_n$	dark-blue needles	1.68			243.0	22.5		+1651.0	6.860[b]
NHP	$[Ni(NH_2NH_2)_5(ClO_4)_2]_n$	purple plates	2.12			220.0			−367.1	8.284[a]

[a] d, density of a material measured by helium-gas pynometry (g·cm^{-3}); Gs, grain size of the crystal (nm); η, crystallinity (%); VoD, theoretical detonation velocity at the measured density and heat of formation (km·s^{-1}); F, friction sensitivity; FOX-7, 1,1-diamino-2,2-dinitroethene; TATB, 2,4,6-triamino-1,3,5-trinitrobenzene. Superscript a: the VoD was calculated by *Explo-5* software by using the literature data. Superscript b: this value was taken from the updated results published by the same group.[14,16]

secondary reaction peaks, in most of the cases, due to a thermite reaction between the decomposition product CuCl (or CuO) and the aluminum sample cell, probably because of the formation of an Al−Cu alloy. This alloy, which melts at exactly at 548 °C (Figure S9),[54] is responsible for the sharp endothermic peaks at 547−549 °C, in all measured DSC thermograms. We can attribute this exothermic peak to a thermite reaction of CuCl with aluminum (Figure S8b).

The results of the TGA measurements were found to be in very good agreement with the DSC findings, where the residues of our ECPs were observed to be over 60%, indicating high Cu contents in the tested materials. The high Cu content was also observed in EA of these ECPs. The initial mass change, with no heat change, could be explained by the loss of crystalline H_2O, included in the cavity of the ECP structures. The mass losses in the main exothermic peaks are in a range of 15.2−42.3%. The mass loss of **ECP-5** in this exothermic process was as low as 15.3% and could be attributed to a relatively low content of the TAG ligand in this material and the presence of CuCl and Cu^0 as impurities. For **ECP-2**, a significant mass loss of about 15.7% was observed, without an obvious heat release below the onset temperature (395 °C), except for a small exothermic peak at 108.1 °C, with an enthalpy of 74 J·g^{-1}.

3.7. Detonation Performance and Mechanical Sensitivity. As shown in Table 1, the densities, measured by helium-gas pycnometry, of all ECPs in this study are much higher (>3.0 g·cm^{-3}) than the density of the parent TAG ligand because of a high Cu content (>30 wt %) and densely packed molecular structures of these ECPs. In terms of the detonation performance, TAG·HCl has a detonation velocity (VoD) of 7198 m·s^{-1}, which is much higher than the VoD values of the TAG-Cu^{I} complex, **ECP-2**, and **ECP-3**, because of the much higher heat of formation of TAG·HCl. Remarkably, **ECP-5** has a VoD value of 8969 m·s^{-1}, which is higher than most of the reported energetic MOFs and insensitive explosives, such as FOX-7 and TATB. In general, we believe that the higher the CuCl content in some of our results in these ECPs, the lower the detonation performance.

The impact and friction sensitivities (I_m) of the TAG-Cu^{I} complex and ECPs were also investigated (Tables 2 and S17). I_m of the complex was found to be 36 J, while the ECPs were found to be *much less sensitive*, with I_m > 98 J. A comparison of the TAG·HCl (I_m = 25 J) impact sensitivity to the sensitivity of the corresponding ECPs shows an interesting phenomenon, where copper coordination causes desensitization of the resulting materials. In comparison, several reported energetic 3D MOFs were found to be more sensitive than **ECP-2**, **ECP-3**, and **ECP-5** [e.g., I_m = 22.5 J for Cu(atrz)] and the very sensitive 1D MOFs (CHP, I_m = 0.5 J) and 2D MOFs (ZnHHP, I_m = 2.5 J; CHHP, I_m = 0.8 J; Table S17). We estimate that the main reasons for the significantly lower mechanical sensitivity of our ECPs are their more rigid framework structures and fewer crystal defects.

4. CONCLUSIONS

In summary, the in situ oxidation and coordination reactions of triaminoguanidine hydrochloride by copper nitrate in aqueous solutions lead to the formation of a series of novel ECPs. The reaction selectivity toward the formation of a specific ECP was easily directed by control of the ratios and concentrations of the reactants and by reaction temperature regime. The best-performing EM obtained in this study was **ECP-5**, which exhibits very low sensitivity (I_m > 98 J), a high VoD of 8969 m·s^{-1}, and a remarkably high decomposition temperature of 396.9 °C. These unprecedented characteristics for EMs represent a new level of balance between two inherently contradicting objectives: high level of the detonation performance versus low level of sensitivity and high thermostability.

■ ASSOCIATED CONTENT

Supporting Information

The Supporting Information is available free of charge on the ACS Publications website at DOI: 10.1021/acsami.6b07165.

Descriptions of the experimental details, characterization techniques, figures of photographs of the as-prepared ECP powders, PXRD and XPS spectra of all involved materials, BSE images of the TAG-Cu^{I} complex, more SEM images of the corresponding screened ECPs, FTIR spectra of the explored materials, oxidation mechanisms of TAG, crystal structures of TAG·HCl, the TAG-Cu^{I} complex, **ECP-2**, **ECP-3**, and **ECP-5**, and DSC curves of other relevant ECPs as well as a Al−Cu phase diagram, tables of a summary of XRD peak parameters, Miller indexing for **ECP-2**, **ECP-3**, and **ECP-5**, results of EA, FTIR and peak assignments, XPS bonding information, and physical properties and performance of our ECPs (PDF)

■ AUTHOR INFORMATION

Corresponding Author

*E-mail: cogozin@gmail.com.

DOI: 10.1021/acsami.6b07165
ACS Appl. Mater. Interfaces 2016, 8, 21674−21682

Present Address
[§]School of Chemistry, Faculty of Exact Science, Tel Aviv University, Tel Aviv, 69978, Israel

Notes
The authors declare no competing financial interest.

■ ACKNOWLEDGMENTS

Financial support from the Planning and Budgeting Committee of the Council for Higher Education in the Israeli government is greatly appreciated. This work was also partially supported by the Center for Nanoscience and Nanotechnology and by the Faculty of Exact Sciences at Tel Aviv University. We are very thankful to Moran Dahan and Dr. Brian Rosen for their valuable contributions to this work.

■ REFERENCES

(1) Krause, H. H. New Energetic Materials. In *Energetic Materials*; Tiepel, U., Ed.; Willey-VCH GmbH & Co. KGaA: Weinheim, Germany, 2005; pp 1−25.
(2) Yan, Q.-L.; Gozin, M.; Zhao, F.-Q.; Cohen, A.; Pang, S.-P. High Energetic Compositions Based on Functionalized Carbon Nanomaterials. *Nanoscale* **2016**, *8*, 4799−4851.
(3) Talawar, M. B.; Jangid, S. K.; Nath, T.; Sinha, R. K.; Asthana, S. N. New Directions in the Science and Technology of Advanced Sheet Explosive Formulations and the Key Energetic Materials used in the Processing of Sheet Explosives: Emerging Trends. *J. Hazard. Mater.* **2015**, *300*, 307−321.
(4) Gaur, B.; Lochab, B.; Choudhary, V.; Varma, I. K. Azido Polymers − Energetic Binders for Solid Rocket Propellants. *J. Macromol. Sci., Polym. Rev.* **2003**, *43*, 505−545.
(5) Yan, Q.-L.; Zeman, S.; Elbeih, A. Recent Advances in Thermal Analysis and Stability Evaluation of Insensitive Plastic Bonded Explosives (PBXs). *Thermochim. Acta* **2012**, *537*, 1−12.
(6) Feng, L.-L.; Cao, D.-L.; Wang, J.-L.; Liu, P.-H.; Zhang, N. Review on Synthesis of Nitroimidazoles Energetic Materials. *Chin. J. Energetic Mater.* **2015**, *23*, 376−385.
(7) Gao, H.; Shreeve, J. M. Azole-based Energetic Salts. *Chem. Rev.* **2011**, *111*, 7377−7436.
(8) Li, Y.; Hao, J.; Liu, H.; Lu, S.; Tse, J. S. High-energy Density and Superhard Nitrogen-rich B-N Compounds. *Phys. Rev. Lett.* **2015**, *115*, 105502.
(9) Huang, X.-C.; Guo, T.; Liu, M.; Wang, Z.-J.; Qiu, S.-J.; Ge, Z.-X. Review on Bis-azoles and Its Energetic Ion Derivatives. *Chin J. Energetic Mater.* **2015**, *23*, 291−301.
(10) Singh, R. P.; Verma, R. D.; Meshri, D. T.; Shreeve, J. M. Energetic Nitrogen-rich Salts and Ionic Liquids. *Angew. Chem., Int. Ed.* **2006**, *45*, 3584−3601.
(11) Comet, M.; Vidick, G.; Schnell, F.; Suma, Y.; Baps, B.; Spitzer, D. Sulfates-based Nanothermites: An Expanding Horizon for Metastable Interstitial Composites. *Angew. Chem., Int. Ed.* **2015**, *54*, 4458−4462.
(12) Tan, B.; Huang, M.; Long, X.; Li, J.; Yuan, X.; Xu, R. From Planes to Cluster: the Design of Polynitrogen Molecules. *Int. J. Quantum Chem.* **2015**, *115*, 84−89.
(13) Wang, J.; Xu, Z.-B.; Meng, Z.-H.; Xue, M. Progress in the Study of Supramolecular Chemistry of Energetic Compounds. *Chin. J. Explos. Propellants* **2015**, *38*, 15−21.
(14) Li, S.; Wang, Y.; Qi, C.; Zhao, X.; Zhang, J.; Zhang, S.; Pang, S.-P. 3D Energetic Metal-organic Frameworks: Synthesis and Properties of High Energy Materials. *Angew. Chem., Int. Ed.* **2013**, *52*, 14031−14035.
(15) Liu, X.; Gao, W.; Sun, P.; Su, Z.; Chen, S.; Wei, Q.; Xie, G.; Gao, S. Environmentally Friendly High-energy MOFs: Crystal Structures, Thermostability, Insensitivity and Remarkable Detonation Performances. *Green Chem.* **2015**, *17*, 831−836.
(16) Zhang, J.; Du, Y.; Dong, K.; Su, H.; Zhang, S.; Li, S.; Pang, S.-P. Taming Dinitramide Anions within an Energetic Metal-Organic Framework: A New Strategy for Synthesis and Tunable Properties of High Energy Materials. *Chem. Mater.* **2016**, *28*, 1472−1480.
(17) Tang, Y.; He, C.; Mitchell, L. A.; Parrish, D. A.; Shreeve, J. M. Potassium 4,4′-Bis(dinitromethyl)-3,3′-azofurazanate: A Highly Energetic 3D Metal-Organic Framework as a Promising Primary Explosive. *Angew. Chem., Int. Ed.* **2016**, *55* (18), 5565−5567.
(18) Bloch, E. D.; Queen, W. L.; Krishna, R.; Zadrozny, J. M.; Brown, C. M.; Long, J. R. Hydrocarbon Separations in a Metal-organic Framework with Open Iron(II) Coordination Sites. *Science* **2012**, *335*, 1606−1610.
(19) Kim, K.; Seo, J. S.; Whang, D.; Lee, H.; Jun, S. I.; Oh, J.; Jeon, Y. J. A Homochiral Metal−organic Porous Material for Enantioselective Separation and Catalysis. *Nature* **2000**, *404*, 982−986.
(20) Kreno, L. E.; Leong, K.; Farha, O. K.; Allendorf, M.; Van Duyne, R. P.; Hupp, J. T. Metal−organic Framework Materials as Chemical Sensors. *Chem. Rev.* **2012**, *112*, 1105−1125.
(21) Bushuyev, O. S.; Brown, P.; Maiti, A.; Gee, R. H.; Peterson, G. R.; Weeks, B. L.; Hope-Weeks, L. J. Ionic Polymers as a New Structural Motif for High-Energy-Density Materials. *J. Am. Chem. Soc.* **2012**, *134* (3), 1422−1425.
(22) Bushuyev, O. S.; Peterson, G. R.; Brown, P.; Maiti, A.; Gee, R. H.; Weeks, B. L.; Hope-Weeks, L. J. Metal-organic Frameworks (MOFs) as Safer, Structurally Reinforced Energetics. *Chem. - Eur. J.* **2013**, *19* (5), 1706−1711.
(23) Li, S.; Pang, S.-P.; Li, X.; Yu, Y.; Zhao, X. Synthesis of New Tetrazene (N−N═N−N)-linked Bi(1,2,4-triazole). *Chin. Chem. Lett.* **2007**, *18*, 1176−1178.
(24) Qi, C.; Li, S.; Li, Y.; Wang, Y.; Chen, X.; Pang, S.-P. A Novel Stable High-nitrogen Energetic Material: 4,4′-Azobis(1,2,4-tri-azole). *J. Mater. Chem.* **2011**, *21*, 3221−3225.
(25) Herres-Pawlis, S.; Neuba, A.; Seewald, O.; Seshadri, T.; Egold, H.; Flörke, U.; Henkel, G. A Library of Peralkylated Bisguanidine Ligands for Use in Biomimetic Coordination Chemistry. *Eur. J. Org. Chem.* **2005**, *22*, 4879−4890.
(26) Zawadzki, H. J. New Coordination Compounds of Copper(II) with Guanidinopyrimidines in N,N-dimethylformamide. *Polym. J. Chem.* **2000**, *74*, 935−944.
(27) Herres-Pawlis, S.; Flörke, U.; Henkel, G. Tuning of Copper(I)-Dioxygen Reactivity by Bisguanidine Ligands. *Eur. J. Inorg. Chem.* **2005**, *19*, 3815−3824.
(28) Herres-Pawlis, S.; Binder, S.; Eich, A.; Haase, R.; Schulz, B.; Wellenreuther, G.; Henkel, G.; Rübhausen, M.; Meyer-Klaucke, W. Stabilization of A Highly Reactive Bis-(μ-oxo)-dicopper(III) Species at Room Temperature by Electronic and Steric Constraint of an Unconventional Nitrogen Donor Ligand. *Chem. - Eur. J.* **2009**, *15* (35), 8678−8682.
(29) Bienemann, O.; Hoffmann, A.; Herres-Pawlis, S. Guanidine-copper Complexes: Structural Variety and Application in Bioinorganic Chemistry and Catalysis. *Rev. Inorg. Chem.* **2011**, *31* (1), 83−108.
(30) Petrovic, D.; Hill, L. M. R.; Jones, P. G.; Tolman, W. B.; Tamm, M. Synthesis and Reactivity of Copper(I) Complexes with An Ethylene-bridged bis(imidazolin-2-imine) Ligand. *Dalton Trans.* **2008**, *7*, 887−894.
(31) Bienemann, O.; Haase, R.; Jesser, A.; Beschnitt, T.; Döring, A.; Kuckling, D.; dos Santos Vieira, I.; Flörke, U.; Herres-Pawlis, S. Synthesis and Application of new Guanidine Copper Complexes in Atom Transfer Radical Polymerization. *Eur. J. Inorg. Chem.* **2011**, *2011*, 2367−2379.
(32) Wang, J.-S.; Matyjaszewski, K. Controlled "Living" Radical Polymerization. Atom Transfer Radical Polymerization in the Presence of Transition-metal Complexes. *J. Am. Chem. Soc.* **1995**, *117* (20), 5614−5615.
(33) Patten, T. E.; Matyjaszewski, K. Atom Transfer Radical Polymerization and the Synthesis of Polymeric Materials. *Adv. Mater.* **1998**, *10*, 901−915.
(34) Andrade, G. R.; Kunsminskas, J.; Pizzuti, L.; Dos Anjos, A.; Inglez, S. D.; Tirloni, B.; Suegama, P. H. Synthesis and X-ray Structural Characterization of Square-pyramidal Copper(II) Complex with

DOI: 10.1021/acsami.6b07165
ACS Appl. Mater. Interfaces 2016, 8, 21674−21682

Aminoguanidine Derivative. *Inorg. Chem. Commun.* **2015**, *61*, 210−213.
(35) Klapotke, T. M.; Mayr, N.; Stierstorfer, J.; Weyrauther, M. Maximum Compaction of Ionic Organic Explosives: Bis(hydroxylammonium) 5,5′-dinitromethyl-3,3′-bis(1,2,4-oxadiazolate) and Its derivatives. *Chem. - Eur. J.* **2014**, *20*, 1410−1417.
(36) Damse, R. S. Studies on the Decomposition Chemistry of Triaminoguanidine Azide and Guanidine Nitrate. *J. Hazard. Mater.* **2009**, *172*, 1383−1387.
(37) Savel'eva, Z. A.; Larionov, S. V.; Ikorskii, V. N. Copper(II) Nitrate Complexes with Di- and Triaminoguanidine and Their Magnetic Properties. *Izvestiya Sibirskogo Otdeleniya Akademii Nauk SSSR, Ser. Khim. Nauk.* **1982**, *2*, 89−92.
(38) Savelieva, Z. A.; Larionov, S. V.; Romanenko, G. V.; Podberezskaya, N. V.; Shishkin, O. V.; Struchkov, Y. T. Coordinated Diaminoguanidinium(1+) Ion in the Crystal Structure of $[Cu(CH_8N_5)Cl_3]$ Complex. *J. Struct. Chem.* **1995**, *36*, 855−859.
(39) Savel'eva, Z. A.; Romanenko, G. V.; Sheludyakova, G. A.; Larionov, L. V. Synthesis and Structure of a Complex with the Coordinated Triaminoguanidinium(2+) ion, $[Cu(TAGH_2)Cl_3]Cl \cdot H_2O$. *Polyhedron* **2000**, *19*, 1737−1740.
(40) Plass, W. Structural Variety and Magnetic Properties of Polynuclear Assemblies Based on 2-Aminoglucose and Tritopic Triaminoguanidine Ligands. *Coord. Chem. Rev.* **2009**, *253*, 2286−2295.
(41) Spielberg, E. T.; Gilb, A.; Plaul, D.; Geibig, D.; Hornig, D.; Schuch, D.; Buchholz, A.; Ardavan, A.; Plass, W. Spin-frustrated Trinuclear Copper Complex Based on Triaminoguanidine with an Energetically Well-separated Degenerate Ground State. *Inorg. Chem.* **2015**, *54*, 3432−3438.
(42) Allen, S. E.; Walvoord, R. R.; Padilla-Salinas, R.; Kozlowski, M. C. Aerobic Copper-catalysed Organic Reactions. *Chem. Rev.* **2013**, *113*, 6234−6458.
(43) Fang, S. W. The Formation of Colored Impurities in Triaminoguanidine Nitrate and Related Incompatibility Problems in Gun Propellants. U.S. Air Force Report AFATL-TR-81-101, Nov 1981.
(44) von Eßen, C.; Christian Göb, R.; Oppel, I. M. Chapter of the Series Topics in Heterocyclic Chemistry, Oct 2015; pp 1−20.
(45) Huerta, L.; Barba-Behrens, N. XPS Characterization of Heterometallic Coordination Compounds with Optically Active Ligands. *J. Chem.* **2013**, *2013*, 1−9.
(46) Graf, N.; Yegen, E.; Gross, T.; Lippitz, A.; Weigel, W.; Krakert, S.; Terfort, A.; Unger, W. E. S. XPS and NEXAFS Studies of Aliphatic and Aromatic Amine Species on Functionalized Surfaces. *Surf. Sci.* **2009**, *603*, 2849−2860.
(47) Yu, J.; Luan, Y.; Qi, Y.; Hou, J.; Dong, W.; Yang, M.; Wang, G. Hierarchical PS/PANI Nanostructure Supported Cu(II) Complexes: Facile Synthesis and Study of Catalytic Applications in Aerobic Oxidation. *RSC Adv.* **2014**, *4*, 55028−55035.
(48) Song, B.-Q.; Qin, C.; Zhang, Y.-T.; Wu, X.-S.; Shao, K.-Z.; Su, Z.-M. The Copper(I) Metal Azolate Framework Showing Unusual Coordination Mode for the 1,2,4-Triazole Derivative and Photocatalytic Activity. *Dalton Trans.* **2015**, *44*, 3954−39583.
(49) Okaya, Y.; Pepinsky, R. Crystal Structure of Triaminoguanidinium Chloride, $(NH_2{\cdot}NH)_3C{\cdot}Cl$. *Acta Crystallogr.* **1957**, *10*, 681−684.
(50) Bracti, A. J. Structure Refinement of 1,2,3-Triaminoguanidinium Chloride, $CH_9N_6^+{\cdot}Cl^-$. *Acta Crystallogr.* **1983**, *C39*, 1465−1467.
(51) Iqbal, P.; Patel, D. S.; Bharatam, P. V. *Ab initio* Study on *N,N′,N″*-Triaminoguanidine. *J. Phys. Org. Chem.* **2007**, *20*, 1072−1080.
(52) Olatta, J. P.; Pitha, J. J. Identification of Salts of Di- and Triaminoguanidine by Powder X-ray Diffraction Methods. *Anal. Chem.* **1952**, *24*, 1187−1188.
(53) Gómez-Gualdrón, D. A.; Moghadam, P. Z.; Hupp, J. T.; Farha, O. K.; Snurr, R. Q. Application of Consistency Criteria to Calculate BET Areas of Micro and Mesoporous Metal-organic Frameworks. *J. Am. Chem. Soc.* **2016**, *138*, 215−224.
(54) Schtirmann, E.; Loblich, H. Phase Boundaries and Interlamellar Spacing in Solidification of the Eutectic System Al-$CuAl_2$. *Metall.* **1977**, *31*, 610−614.

DOI: 10.1021/acsami.6b07165
ACS Appl. Mater. Interfaces 2016, 8, 21674−21682